Journal of Alloys and Compounds 1002 (2024) 175385

Contents lists available at ScienceDirect

Journal of Alloys and Compounds

journal homepage: www.elsevier.com/locate/jalcom

Ultra-selective hydrogen sensors based on CuO - ZnO hetero-structures grown by surface conversion

Barnika Chakraborty [a,1], Dinu Litra [b,1], Abhishek Kumar Mishra [c,*], Cristian Lupan [b], Rajat Nagpal [b], Soni Mishra [d], Haoyi Qiu [a], Serghei Railean [b], Oleg Lupan [a,b,e,**], Nora H. de Leeuw [f,g], Rainer Adelung [a,h], Leonard Siebert [a,h,**]

[a] Chair for Functional Nanomaterials, Department for Material Science, Kiel University, Kaiserstr. 2, Kiel D-24143, Germany
[b] Center for Nanotechnology and Nanosensors, Department of Microelectronics and Biomedical Engineering, Technical University of Moldova, 168 Stefan cel Mare str., Chisinau MD-2004, Republic of Moldova
[c] Department of Physics, Applied Science Cluster, School of Advanced Engineering, University of Petroleum and Energy Studies (UPES), Bidholi via Premnagar, Dehradun, Uttrakhand 248007, India
[d] Department of Physics, Graphic Era Hill University, Dehradun 248002, India
[e] Department of Physics, University of Central Florida, Orlando, FL 32816-2385, USA
[f] School of Chemistry, University of Leeds, Leeds LS2 9JT, United Kingdom
[g] Department of Earth Sciences, Utrecht University, Princetonplein 8A, Utrecht 3584 CD, the Netherlands
[h] Kiel Nano, Surface and Interface Science - KiNSIS, Kiel University, Kiel, Germany

ARTICLE INFO

Keywords:
Sensors
Morphology
Zinc oxide
Copper oxide
Heterostructures
Surface conversion

ABSTRACT

Synergistic effects of mixed oxides have the potential to improve sensing performances of environmental, domestic and industrial monitoring devices. However, mixed oxides often come in the form of separate particles and are thus addressed separately by the environment, instead of capitalizing on the interface between the metal oxides. This paper describes a new core@shell gas sensing material of tetrapodal zinc oxide with a surface coating of crystalline copper oxide(t-ZnO@CuO). The special surface conversion strategy yields a unique, self-assembled and pinhole-free coating of CuO nanoplatelets. The morphologies, structural, chemical and gas sensing properties of the heterostructure were investigated. To evaluate the sensing properties of the heterostructure, t-ZnO@CuO was fabricated as nanosensors, consisting of one core-shell rod of CuO-coated crystalline ZnO. The single core@shell rod showed high selectivity towards hydrogen already at comparatively low operation temperatures of 150 °C. Computational calculations based on the density functional theory (DFT) have been carried out to understand the interaction of the H_2 gas molecule with the surface of the CuO nanostructures. The surface conversion was done wet chemically and is a novel method for generating heterostructures that can be potentially transferred to heterojunctions with unique properties for chemosensors.

1. Introduction

Gas sensors made of metal oxides have attracted attention in society for monitoring gases in fields like medicine, industry, food, automotive, agriculture, and household applications [1–3]. The modern trend of developing small, solid state gas detectors with low power consumption has led to the development of semiconducting oxides as excellent candidates to fabricate highly sensitive and miniaturized gas sensors [4]. Furthermore, to increase the sensitivity of metal oxide gas sensors, they can be interfaced with each other to form heterojunctions [5,6]. In this regard, the highly efficient and unique morphology of 3D networks of interconnected tetrapodal ZnO (t-ZnO) with excellent optical properties [7] and fast response was fabricated [8,9]. However, due to the large dimensions of tetrapodal networks (~1–10 μm) low sensitivity was observed in gas sensing performance [8].

Hydrogen is an environmental component that requires monitoring

* Corresponding author.
** Corresponding authors at: Chair for Functional Nanomaterials, Department for Material Science, Kiel University, Kaiserstr. 2, Kiel D-24143, Germany.
E-mail addresses: akmishra@ddn.upes.ac.in (A.K. Mishra), cristian.lupan@mib.utm.md (C. Lupan), ollu@tf.uni-kiel.de, oleg.lupan@mib.utm.md (O. Lupan), lesi@tf.uni-kiel.de (L. Siebert).
[1] These authors contributed equally.

https://doi.org/10.1016/j.jallcom.2024.175385
Received 22 February 2024; Received in revised form 20 June 2024; Accepted 27 June 2024
Available online 1 July 2024

in household and energy applications [10,11]. Hydrogen detection has become of vital importance, especially after the Industrial Revolution due to its diverse applications in fields like fertilizer production [12], petrochemical industries [13], electricity production [14], and metal galvanization [15]. For example, battery rooms should be cautiously ventilated to limit the hydrogen concentration to < 4 % to maintain its Lower Explosive Limit (LEL), in accordance with European standards as per CENELEC BS EN 50272-1:2010 [16]. Nowadays, hydrogen attracts even more attention as a promising renewable energy fuel and will therefore likely be used in more applications in the near future [17,18]. There are lot of studies reported on hydrogen sensors [19], but the current work shows good selectivity and long term stability which can be applied in a wide range of industries and environments where hydrogen monitoring is critical, including hydrogen fuel production, storage, transportation, and utilization, as well as industrial processes, environmental monitoring, and safety applications [20,21].

Therefore, more effective and sensitive detection of hydrogen in the environment is highly important for the safe production, storage and utilization of hydrogen. Metal oxide semiconductor sensors change their conductivity upon exposure to reducing or oxidizing gases but they are typically not capable of selecting which gases are being measured. The electrical characteristics of a sensing material can be analyzed based on the electron transfer and interactions occurring between the surface and adsorbed gas molecules [22]. The adsorption capacity of gas sensors varies as a function of temperature, and the resistance is typically recorded when voltage/current changes occur. There are many methods to improve sensory properties such as doping, fusing or polymer deposition [23]. An effective fabrication of *p-n* heterojunctions leads to charge transfer through an interface to attain Fermi level equilibrium on both sides, which results in modulation of conductive channels on the sensing surface [23,24]. Shell layer as in CuO plays another important role through its catalytic action for decomposition of certain gases which contributes to improvement in sensing performance [25]. Copper oxides are known for *p*-type semiconducting behavior [26–28] since they are metal-ion-deficient, and the majority of charge carriers are holes ($h+$) [29,30]. From another side, zinc oxide possesses *n*-type conductivity behavior since they have oxygen-vacancy (VO) donors obliged for *n*-type conductivity, and the majority of charge carriers are electrons ($e-$) [26,31].

To improve the gas sensing characteristics of 3D t-ZnO networks [8], in this study, a novel interface is created by directly reacting the surface of the t-ZnO particles with a copper salt solution by a novel approach. This creates core@shell structures of t-ZnO@$Cu(OH)_2$ which can be subsequently dehydrated to t-ZnO@CuO. In these particles, the interface or heterojunction is sandwiched between the inner ZnO core and the outer CuO layer. This type of interface sensor was tested for its sensitivity towards hydrogen, ethanol, methane, n-butanol, 2-propanol, acetone, carbon monoxide, hydrogen sulfide and ammonia. It was shown that the t-ZnO@CuO interface improves hydrogen sensing performance due to potential barrier modulation at the heterojunction interface and low dimension (~800 nm CuO layer) over the t-ZnO surface.

2. Materials and methods

2.1. t-ZnO synthesis

The tetrapodal zinc oxide (t-ZnO) particles in this study were synthesized utilizing a flame transport synthesis as described in our previous works [8,32]. For this process zinc particles with a size of 5 μm were added to polyvinyl butyral (PVB) powder (Kuraray Europe GmbH, Germany), at a weight ratio of 1:2. The mixture was then heated in an alumina crucible using a preheated oven set to 900 °C. This increase in temperature started a reaction of the PVB with the surrounding oxygen protecting the zinc particles from oxidation until their evaporation occurred. In the gaseous phase, the zinc started to form nuclei which subsequently developed into tetrapodal-shaped microcrystals. After 30 min the crucible was taken out of the oven and the t-ZnO could be collected as white fluffy powder.

2.2. t-ZnO@CuO synthesis

The t-ZnO was coated with a metal derivative to form a core@shell structure of ZnO@$Cu(OH)_2$ by wet chemical synthesis at room temperature. A concentration of 0.1 M solution of $CuSO_4$ acts as the precursor. T-ZnO is added to the precursor at a concentration of 1 mg/mL for approximately 2 h, which produces a uniform coating of $Cu(OH)_2$ in a self-organized pattern on ZnO which is very stable over time. The solution is then washed with water and dried in the vacuum oven at 70 °C. The next step involves the treatment of t-ZnO@$Cu(OH)_2$ with H_2O_2 over 1 h at room temperature to obtain t-ZnO@CuO. The conversion can be marked easily by the change in color from bluish-green to black. The solution is also further rinsed with water and dried.

2.3. Electron microscopy

The morphology and geometry of the sample were investigated by scanning electron microscopy (SEM) REM- ZEISS (7 kV, 10 μA). The prepared powdered sample was directly attached in minute quantity with the help of carbon tape on the SEM stab for measurements. Transmission energy microscopy (TEM) was performed using the Tecnai F30 microscope. The samples for TEM analysis were prepared by grinding them and having a pinch of the sample of Ni grid. Cu grid was avoided as the sample already contained CuO in it.

2.4. Raman characterization

In order to further determine the formation of CuO on ZnO structure, chemical analysis of the prepared samples was conducted using micro-Raman spectroscopy in ambient conditions. A WITec Alpha300 RA system (WITec GmbH, Ulm, Germany) equipped with a triple grating spectrometer and a CCD detector was used, where the grating parameters were set at 600 g/mm with a blaze wavelength of 500 nm. The excitation source was a green laser with a wavelength of 532 nm. Prior to the investigations, the spectrometer was calibrated using a Si wafer.

2.5. XRD structure analysis

A primary structural characterization was performed by Rigaku Smartlab X-ray powder diffraction (XRD) operating at 40 kV and 40 mA, with $CuK_{\alpha 1}$ radiation ($\lambda = 1.54$ Å) over a range of 20–80°. The signals obtained proved the crystalline nature of the samples. The measurement was performed on a non- metallic holder in order to avoid noise from the holder.

2.6. The gas sensors fabrication and measurement

The nanosensors were made in a FIB/SEM dual beam set-up as reported in our previous works [33]. In summary, the individual rods of t-ZnO@CuO were placed on a silicon oxide/silicon wafer with deposited gold contacts of 180 nm. Then, the rods were contacted by depositing the platinum complex with a focused ion beam FIB/SEM dual beam. These contacts were nano-welded to both the gold substrate and the tip of the t-ZnO@CuO rods.

Gas detection characteristics were obtained using the Keithley 2400 as the source and measurement device. The characteristics of this device are to apply and measure voltage and current with very high accuracy. It was connected to a personal computer for data transfer. The acquisition and storage of experimental data were done using LabView software (from National Instruments) [28]. The sensor chamber consists of a heater as a substrate connected to the power supply, the probes for connecting the sensor surface to the Keithley 2400 sourcemeter, and the

gas pipe connected to a system of pumps and valves connected to the gas tank with different concentrations in this case 50 ppm, 100 ppm, 500 ppm at the time of the experiment the atmospheric humidity was about 10 %.

2.7. Computational details

Our calculations are based on Density Functional Theory (DFT) methods, employing the plane-wave approach [34–36] as implemented in the Vienna Ab-initio Simulation Package (VASP) [37]. We used the projector augmented wave (PAW) method to describe the interactions between ions and electrons [38], and the Perdew–Burke–Ernzerhof functional [39] was used for the non-local exchange-correlation energy. The tetrahedron method with Blöchl correction [40] was used to optimize the atomic structures and the optimized structures were obtained by fully relaxing the positions of all the atoms until the atomic forces on each ion were less than 0.01 eV/Å. We used a 5 × 5 × 1 Monkhorst–Pack [41] k-point mesh to simulate the heterostructures. Other details are the same as in our earlier works [42–44]. In order to incorporate the long-range dispersion forces between molecules and surfaces, we employed the DFT-D3 approach as described by Grimme [45]. Atomic charges were obtained through the Bader analysis [46]. Through DFT calculations, as reported in Section 2.4, the heterostructure 2, consisting of two Cu atoms on the ZnO surface shows better interaction with the H_2 gas molecule compared to Heterostructure 1 where we had only 1 Cu atom. This is also reflected in our charge transfer plots representing the increase in sensitivity for gas molecules with an increase in Cu-O bonds over the ZnO surface.

3. Results and discussion

3.1. t-ZnO@CuO core@shell particles

3.1.1. Morphological, structural and chemical analysis of t-ZnO@CuO

The t-ZnO@CuO sensors are made by directly reacting the surface of t-ZnO with copper sulfate solution. This treatment leads to the formation of copper hydroxide ($Cu(OH)_2$), which can be subsequently transformed to copper oxide by thermal annealing, thus creating one joint interface. In Fig. 1, SEM images of both t-ZnO@$Cu(OH)_2$ and t-ZnO@CuO particles based on a tetrapodal morphology are presented. It was observed that on the surface of the t-ZnO, $Cu(OH)_2$ nanostructures have been deposited evenly, as shown in Fig. 1**b-d**. The size of the layers of $Cu(OH)_2$ around ZnO is approximately 800 nm. The layers are self-organized and tightly bound to the surface of t-ZnO. However, when dehydrated to CuO form, the flake structures become larger. The difference in the texture of the outer layers can be seen from the SEM images. The study of the morphology via TEM yielded the presence of CuO nanoplatelets on the t-ZnO.

The novelty of this experiment lies in the unique surface conversion strategy, the resulting superior hydrogen sensing performance, and the comprehensive understanding achieved through both experimental and computational methods. This paves the way for further development and optimization of highly sensitive and selective hydrogen sensors [24] based on individual core@shell structures, like microrods or heterojunctions *p-n*. We showed a self-organized growth of nanostructures of copper hydroxide and its subsequent conversion to copper oxide on single-crystalline ZnO microrods and their application as ultra-selective H_2 gas sensors. The selectivity of these structures for H_2 gas sensors is unique due to *p-n* type heterojunction between copper oxide and zinc oxide [42,47]. The initial self-organized growth method and the resulting, pinhole-free and homogeneous thickness of the $Cu(OH)_2$ platelets on top is unique as well and opens up the field for a novel class of composites with core@shell structures of two semiconducting

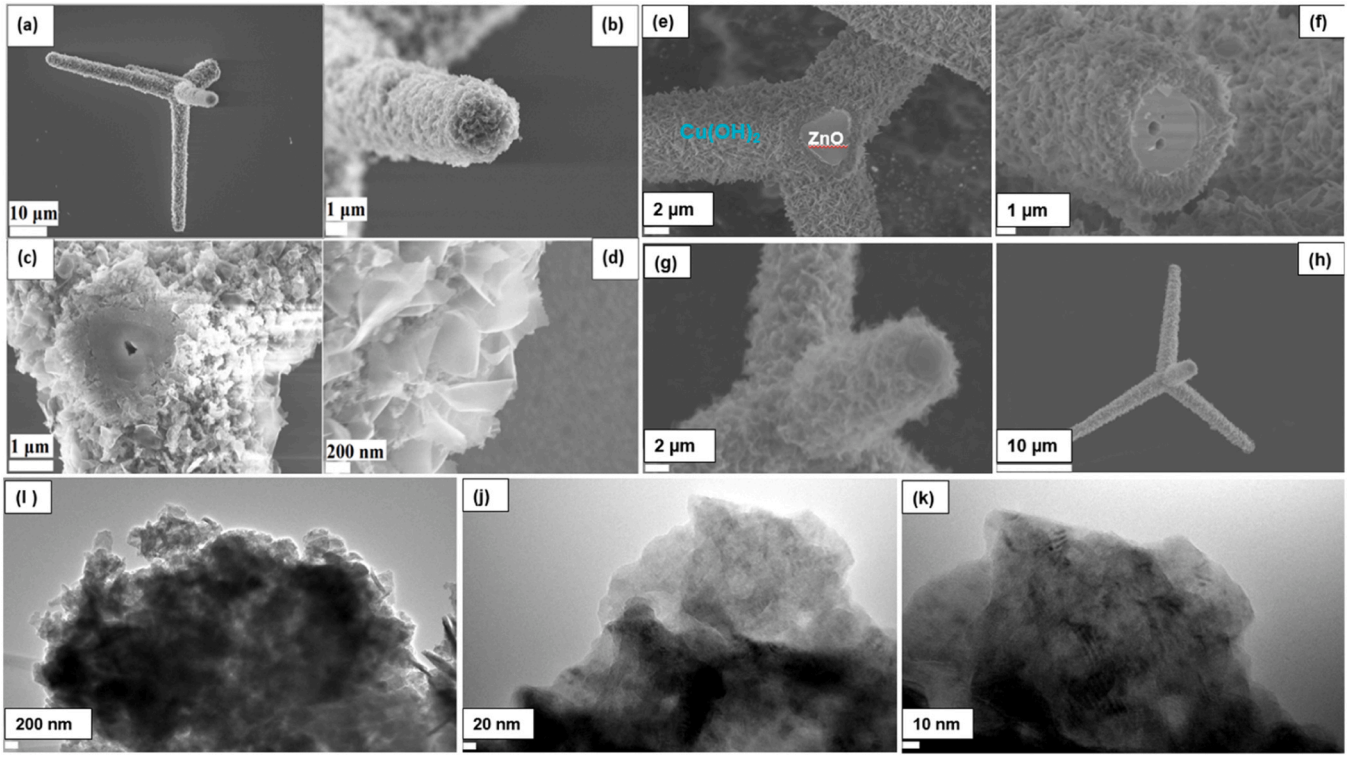

Fig. 1. SEM images of t-ZnO@CuO nanosensors based on coated t-ZnO: (a) individual t-ZnO@CuO, (b,c,d) the surface of t-ZnO@$Cu(OH)_2$ at different magnification. (e,f) $Cu(OH)_2$ layer deposited uniformly on t-ZnO and leaving the core of ZnO intact. (g,h) CuO layer on t-ZnO after treatment with H_2O_2 at different magnifications. (i, j, k) TEM bright field images of ZnO@CuO microparticles at varying magnifications showing the crystal planes and a polycrystalline structure.

materials in a rod-like arrangement.

In Fig. 2, the structural and vibrational studies are presented. In the structural analysis, the crystalline t-ZnO core reflects the hexagonal crystal structure with space group $P6_3mc$. Diffractions obtained at a 2Θ value of 31.6°, 34.5°, 47°, 56.95°, 63.4°, 66.3° stands for (010), (002), (012), (110), (013), (020) planes respectively (Reference File: 98–000–9340). As part of the shell or outer layer to nucleate on ZnO an attempt to prepare copper oxide gave two phases of the latter. CuO was deposited as Monoclinic crystal system with space group C2/c. Diffractions were obtained indicating CuO at 2Θ values of 32.5°, 35.65°, 45.9°, 48.7°, 67.6° which correspond to the (110), (11−1), (11−2), (20−2), (113) planes, respectively (Reference File: 98–000–5750). Additionally, another phase of Cu_2O is also observed. Diffractions obtained corresponding to Cu_2O at 29.9°, 37.05°, 62.35° reflects the (110), (111), (220) planes, respectively. The broader diffractions of t-ZnO@-CuO indicate a certain degree of amorphization of the CuO platelets.

Fig. 2**b** presents the Raman spectrum of the t-ZnO@CuO sample, where the measuring point is indicated in the inserted microscopic image. The sample exhibits the typical peaks for CuO (B_g) and ZnO (E_2 and $2A_1$(LO)) reported in the literature [48–50], which indicates successful deposition of CuO on t- ZnO. An additional peak for Cu_2O was found, corroborating the finding of the corresponding diffractions in XRD.

3.1.2. Sensor fabrication of t-ZnO@CuO

In Fig. 3 SEM images of nanosensors made from individual arms of the CuO-covered t-ZnO shell@core are presented. The microwires/rods were obtained by crushing the tetrapodal crystals on SiO_2/Si substrates. It is important to mention that CuO is a *p*-type semiconductor oxide and ZnO is with a *n*-type, thus forming a *p-n* junction at their interface or heterojunction [26–28,42,47]. They are placed between the gold contacts which makes connection and subsequent testing possible. The microwires have different lengths, but similar diameters of ~3–4 μm. Fig. 3**c** depicts a nanosensor based on two t-ZnO@CuO microwires of different lengths. Similar to the tetrapod morphology, it was observed that CuO was evenly deposited on the microwire's surface.

3.1.3. Sensor characterization of t-ZnO@CuO core@shell

The response to case *S* was calculated using the values of the currents and voltage measured when the nanostructures were exposed to air and gas, respectively. Thus, the formula was used to determine the gas response in percent [51]:

$$S = \frac{G_{gas} - G_{air}}{G_{air}} * 100\% \quad (1)$$

where G_{gas} is the electrical conductance of the sensor measured when exposed to gas and G_{air} is the electrical conductance measured when exposed to air [43,52].

Fig. 4 represents the dynamic response of t-ZnO@CuO nanosensors to 50 ppm, 100 ppm and 500 ppm hydrogen at the operating temperatures of 150 °C and 175 °C. The maximum response value obtained was S =520 at the operating temperature of 175 °C and the concentration of 500 ppm. The response time is the time interval in which the increase of the S value from 10 % to 90 % takes place, being approximately 17 s, and the recovery time, i.e. the time interval in which the decrease of the S value from 90 % to 10 % takes place, is approximately 89 s. A voltage of 25 V was applied for 20 s then the gas flow impinges on the nanosensor surface which leads to the enhancement in electrical current flow. Higher sensing response at 175 °C over 150 °C can be ascribed to Langmuir adsorption theory, which suggests that the adsorption rate is better at the former temperature than the latter. The given sensors were measured at an operating temperature of up to 175 °C due to the device limit. This increase in recovery time with increasing operating temperature is ascribed to the dominance of the Arrhenius expression for electrical conductivity [11] over oxygen site reduction which clearly depicts an increase in electrical conductivity with an increase in operating temperature. The comparative study with all the other reported studies is as shown in Table 1.

Cyclic and long-term stability were also investigated. Fig. 5 shows the cyclic stability, where 3 pulses were applied in a row, and a small increase of the response was observed between the pulses. This is due to the fact that the nanostructures did not recover after the pulse, the decision was to give a longer time for recovery of the signal, but the amplitude of the pulses is the same, i.e. the same response value, which demonstrates the cyclic stability.

In Fig. 6, it shows the hydrogen response at 100 ppm concentration at 10 % and 50 % humidity for comparison. It shows the decrease in hydrogen response by increasing relative humidity from 10 % to 50 %. One explanation is the quadrupling of H_2O molecules on the surface of the nanostructures by occupying ionic oxygen adsorption sites [53–55] and the subsequent blocking of the hydrogen molecules.

Fig. 7 shows the good selectivity toward H_2 gas and its excellent sensing performance which is ascribed to the *p-n* heterojunction effect of the core@shell structure, which leads to better charge separation and therefore to the excellent sensing performance. Fig. 7 shows the

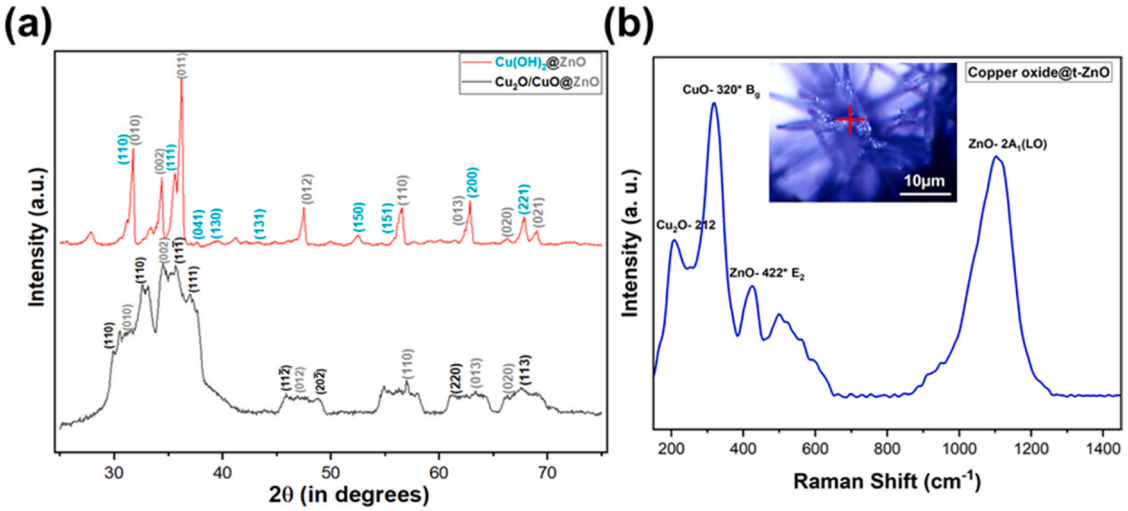

Fig. 2. (a) Two X-ray diffraction patterns of copper hydroxide-coated t-ZnO and copper oxide-coated t-ZnO, converted from copper hydroxide. (b) The Raman spectrum of the t-ZnO@CuO tetrapod.

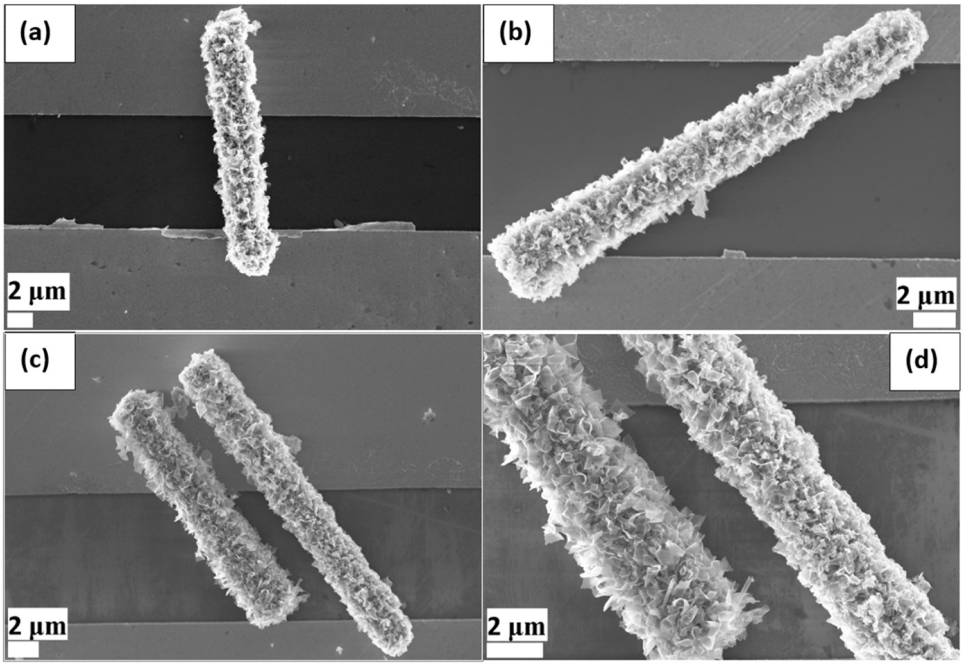

Fig. 3. SEM images of t-ZnO@CuO nanosensors: (a,b) single microwire, (c) two microwires at lower magnification, (d) two microwires at higher magnification.

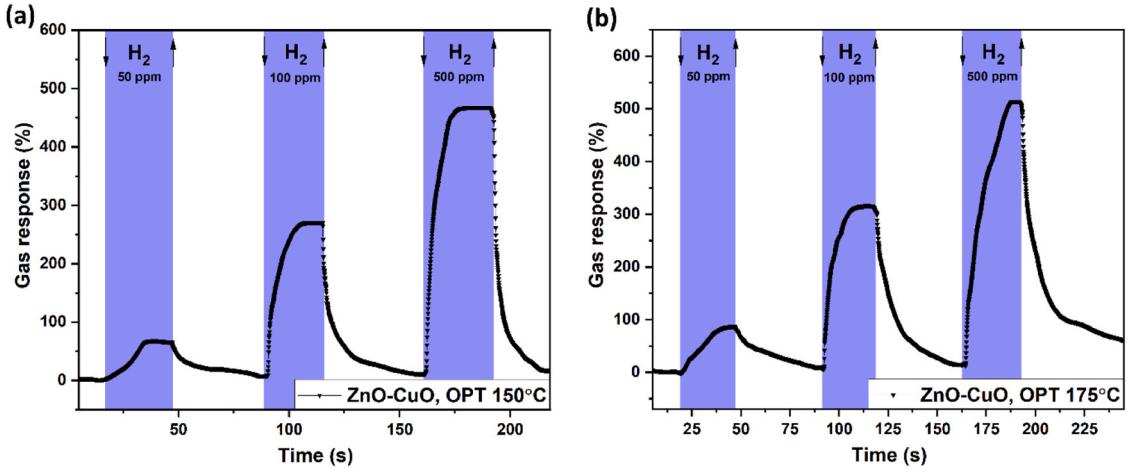

Fig. 4. Dynamic response to hydrogen with a concentration of 50 ppm, 100 ppm and 500 ppm at operating temperature of (a) 150 °C and (b)175 °C.

Table 1
Table for comparative reported study with current work.

Sensing structure and morphology	Preparation method	Target gas concentration (ppm)	Operating temperature (℃)	Hydrogen response (%)	Response/recovery time (s)
ZnO/CuO bi-layer heterostructures [57]	Chemical solution	100	200	~138	-
Single ZnO nanorod [72]	Hydrothermal	200	25	~4	30/90
Single ZnO nanowire [73]	Chemical vapour phase growth	100	25	~35	64/11
CuO:Zn/Cu_2O:Zn [28]	Chemical synthesis from solutions	100	200	~95	-
CuO/ZnO heterojunctions [74]	Subsequent thermal annealing	1000	25	~4	~92/2
TiO_2/CuO:Zn [75]	Synthesis from chemical solution	100	200	~110	-
t-ZnO@CuO core shell (single or two microrods) (This work)	Wet chemical	100	175	~320	~17 /89

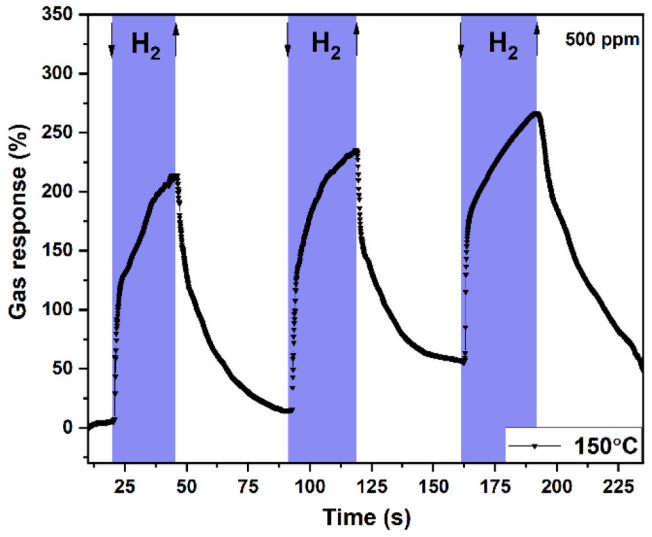

Fig. 5. Dynamic response to hydrogen with a concentration of 500 ppm at operating temperature of 150 °C.

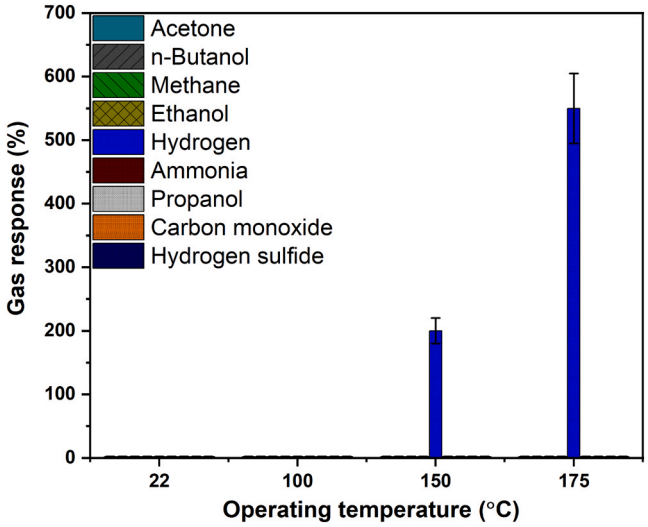

Fig. 7. Response to gases with a concentration of 100 ppm and different operating temperature of t-ZnO@CuO single microrod-based sensors.

influence of operating temperature on the sensitivity of sensing response. By increasing temperature, hydrogen sensing response increases due to the availability of sufficient adsorbed ionic species of oxygen on the surface which will react much more efficiently with hydrogen molecules at higher temperature [56,57]. However, recovery time increases as we move from and operating temperature of 150 °C to 175 °C which shows the desorption rate deteriorating at higher temperatures.

Fig. 8 shows long-term stability, in total 3 measurements per each experiment were performed with a difference between them of 120 and 240 days. From the obtained graph it can be observed a decrease in the sensitivity over time, one of the supposed causes would be the degradation of the copper oxide nanostructures on the surface due to their heating at each measurement. These results clearly indicate the direction to continue research in this field with the aim of improving the stability over time as well as sensor performances by control of t-ZnO@CuO interface and nanoscale *p-n* heterojunctions.

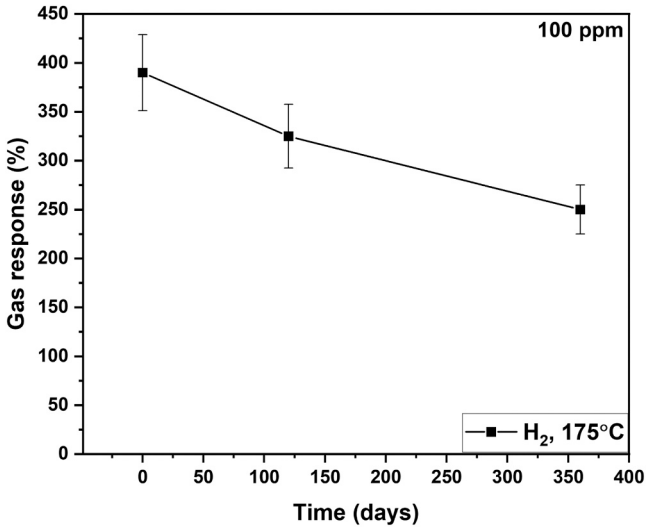

Fig. 8. Long term stability response to hydrogen with a concentration of 100 ppm at operating temperature of 175 °C.

3.2. Gas sensing mechanism

In the general sensing mechanism, oxygen molecules adsorb on the surface of semiconducting metal oxides and transform into ionic species (O_2^-, O^-, and O^{2-}) at different operating temperatures by capturing

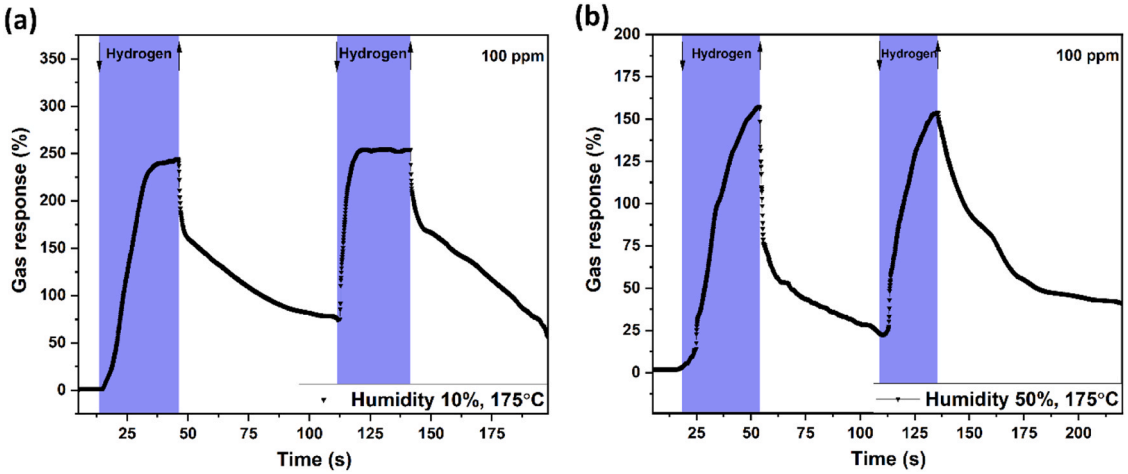

Fig. 6. Dynamic response to hydrogen with a concentration of 100 ppm at operating temperature of 175 °C and humidity of (a) 10 % and (b) 50 %.

electrons from the semiconductor's surface [58–60]. The transformed ionic species depend upon the operating temperature, e.g. for < 200 °C mono-ionized molecular oxygen ions (O_2^-) may exist; in the temperature range 200 °C - 550 °C, mono-ionized oxygen atoms (O^-) may exist, and at temperatures > 550 °C, double ionized oxygen atom mays exist [61,62]. These charged species lead to band bending at the surface of the semiconductor oxide and form a space charge region with either a hole accumulation layer (*p*-type semiconductor) or an electron depletion layer (*n*-type semiconductors) [24]. The former becomes more conductive, *p*-type, the latter (*n*-type) less conductive when oxygen ions adsorb on the surface.

Next, reducing gases react with the oxygen ions on the surface of the metal. The ionic oxygen species release the trapped electrons back into the conduction bands of the metal oxide (i.e. ZnO, an *n*-type semiconductor) and the device's electrical resistance decreases [63]. The hydrogen detection mechanism at temperatures < 200 °C can be understood well with the help of the following equations [64]:

$$O_{2(ads.)} + e^- \rightarrow O^-_{2(ads.)} \quad (2)$$

The higher the temperature, the more easily the oxygen can be ionized [65]. Therefore, at temperatures over 400 °C, oxygen species like O^{2-} are adsorbed on the sensing surface, which will be different from the O_2^- oxygen species produced at 150 °C or 175 °C operating temperatures. The hydrogen detection mechanism at a temperature of 150 °C or 175 °C can be understood well with the help of the following equations for *p*-type and *n*-type semiconducting oxides [66]:

$$2H_{2(gas)} + 4h^+ \leftrightarrow 4H^+_{(ads)}, \quad (3)$$

$$4H^+_{(ads)} + O^-_2 \leftrightarrow 2H_2O \quad (4)$$

So, new *p*-*n* heterojunctions really help to eliminate the disadvantages of semiconducting oxide nano-micro-structures such as the poor selectivity between gases, which is a serious disadvantage of semiconducting oxide based nanosensors, since a single nanomaterial based nanosensor cannot identify properly a specific gas species. Due to the interface effect of the heterojunction [24], the sensing performance of developed is improved even more, namely for a mixed oxide of ZnO and CuO (e.g. t-ZnO@CuO), the electrical resistance at grain interfaces is reduced to half its value, irrespective of the nature of the target gas [24, 67] The main point, however, is that the target gas can reach the reactive interface and vary the surface charge density at the interface [67], which then leads to the sensing response activity. Increasing the amount of CuO typically leads to an increase in sensitivity to H_2 gas [24,68,69]. This is because a higher concentration of CuO provides more active sites for the interaction between H_2 molecules and the sensor surface [24]. As a result, there is a greater probability of H_2 molecules reacting with the surface, leading to a more pronounced change in electrical conductivity and thus a higher sensitivity of the sensor to H_2 [24,69]. For this structure, the complete coverage of CuO on the t-ZnO arm may prevent the diffusion of larger molecules like methane or propane to the interface. Hydrogen, however, is so small, that it is the only diffusible species and can therefore penetrate shell of t-ZnO@CuO heterostructure and react at the interface. Another explanation may be that the macromolecules like ethanol, acetone, etc. generally do not show a high gas response at these low temperatures [70,71]. Therefore, an excellent sensitivity of t-ZnO@CuO towards H_2 over other VOCs like acetone, ethanol, propanol, carbon monoxide and hydrogen sulfide or *n*-butanol can be ascribed to both the moderate sensing temperature (175 °C), and the high hydrogen gas diffusivity.

3.3. Computational analysis

In our study, we initiated calculations based on a previously simulated ZnO $(10\bar{1}0)$ surface structure, which has been identified as the most reactive surface for ZnO [42–44]. The top layer of this ZnO (10−10) surface comprises two distinct types of Zn atoms: Zn1 and Zn2. Notably, Zn1 atoms are more exposed compared to Zn2 atoms (as depicted in Fig. A1). To create t-ZnO@CuO heterostructures, we replaced the top surface Zn atoms with Cu atoms. Specifically, we introduced a single Cu atom into the ZnO (10−10) surface, effectively substituting it for the most exposed Zn atoms. After performing geometry optimization, the Cu atom forms bonds with three O atoms. It binds to one of the most exposed O atoms at a distance of 1.852 Å, while the other two less exposed O atoms exhibit bond lengths of 1.94 Å. This resulting structure is denoted as the Hetero1 structure and is illustrated in Fig. 9.

In our investigation of t-ZnO/CuO heterostructures, we introduced Cu atoms by replacing two Zn atoms on the ZnO (10−10) surface. We explored two distinct configurations:

Configuration 1: We substituted two neighboring exposed Zn atoms in the top surface layer.

Configuration 2: We replaced one Zn atom from the top layer and another Zn atom from the sub-surface layer.

After relaxation, we found that Configuration 1, where we replaced two adjacent exposed Zn atoms, exhibited lower energy. Similar to the Hetero1 structure, Cu atoms formed bonds with the one of the most exposed O atoms (dCu-O = 1.84) and two sub-surface O atoms (dCu-O = 1.869, 2.008 A), as shown in Fig. 9 (Hetero2).

We next investigated the interaction of an H_2 gas molecule with these two t-ZnO/CuO heterostructures. First, we investigated the Hetero1 structure with one substitutional Cu atom by placing the H_2 molecule in different orientations close to the Cu-O bonds, where we found that the H_2 molecule interacts with the Cu atom by attaching atomically to the surface [Fig. 10]. One of the H atoms binds to Cu with a Cu-H bond of 1.501 Å and, as a result, the Cu atom moves upwards to cause elongation of one of Cu-O surface bonds to 1.966 Å. The second H atom binds to a nearby top oxygen atom at a distance of 0.979 Å. The calculated interaction energy was found to be −61.63 kJ/mol.

We further investigated the interaction between an H_2 gas molecule and the Hetero2 structure, which contains two substitutional Cu atoms. Our results reveal that the H_2 molecule dissociates atomically upon interaction, as illustrated in Fig. 10. Compared to other configurations, the interaction with the Hetero2 structure exhibited greater strength, characterized by a binding energy of −114.82 kJ/mol. In this heterostructure, one of the hydrogen atoms forms bonds with both Cu atoms present on the surface. The Cu-H bond lengths were measured at 1.549 Å and 1.600 Å. Simultaneously, the second hydrogen atom binds to a nearby oxygen atom with a bond length of 0.976 Å. This enhanced interaction with the Hetero2 structure suggests that the presence of t-ZnO/CuO moieties enhances the structure's affinity for the H_2 molecule.

To gain deeper insights into the charge distribution during interaction, we conducted a Bader charge analysis. The results, presented in Fig. 11, indicate that the hydrogen atom binding with both Cu atoms acquires a positive Bader charge of +0.66. Conversely, the hydrogen atom bonded to the surface oxygen atom displays a negative Bader charge of −0.083.

4. Conclusions

In summary, this study investigates gas sensors utilizing mixed oxides of tetrapodal t-ZnO and CuO, with CuO deposited as nanoplatelets through a surface conversion reaction of t-ZnO. A perfect coating of amorphized nanoplatelets of CuO on t-ZnO microrods was obtained. The resulting core@shell material, employed in a single microrod sensor configuration, exhibits remarkable sensitivity to hydrogen, showcasing selectivity. Through DFT calculations, mechanistic insights into the formation of t-ZnO@CuO nanostructures and their interaction with H_2 molecules were gained, highlighting the enhancement of interaction due to the presence of t-ZnO@CuO moieties. Operating at 175°C, the sensor demonstrates a gas response of approximately 520 % towards 500 ppm of H_2, with exclusive sensitivity to hydrogen, affirming its high

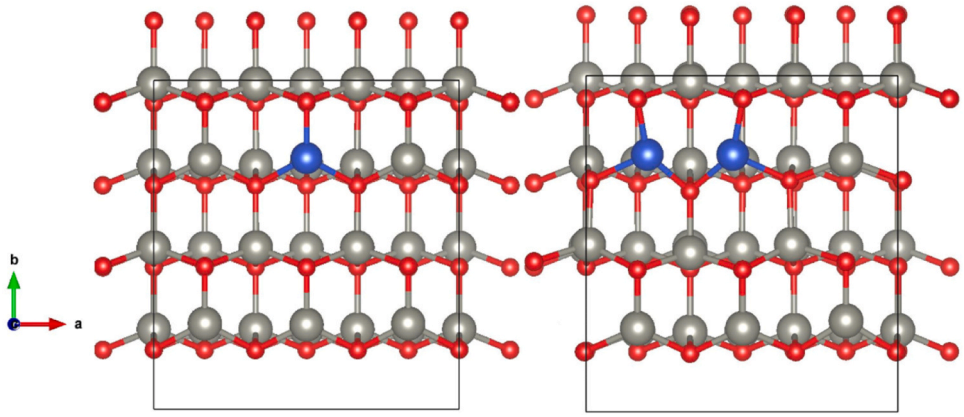

Fig. 9. Top views of Hetero1 (One Cu atom substituted in the ZnO $(10\bar{1}0)$ surface) (left) and Hetero2 (Two Cu atoms substituted in the ZnO (10−10) surface) (right) heterostructures. Zn and O atoms are shown by grey and red coloured balls, respectively, while blue coloured balls depict Cu atoms.

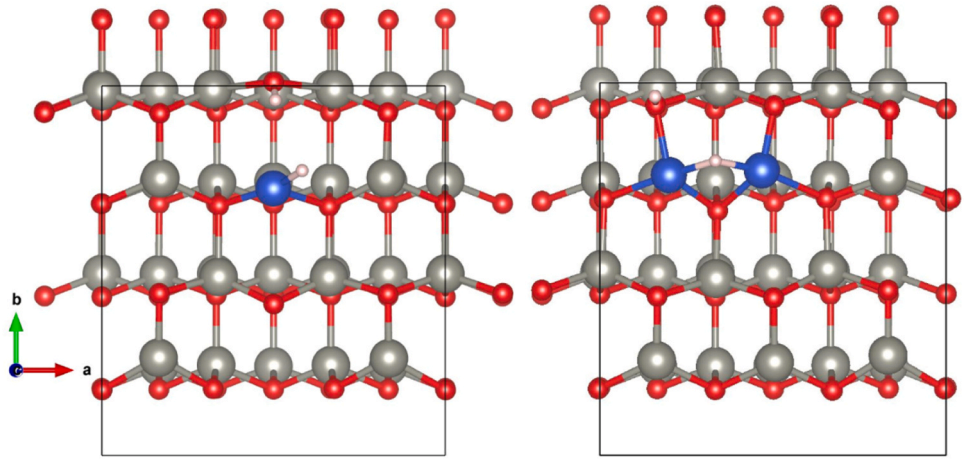

Fig. 10. Top views of the interaction of the H_2 molecule with the Hetero1 (one substitutional Cu atom on the ZnO $(10\bar{1}0)$ surface) (left) and Hetero 2 (two substitutional Cu atoms on the ZnO (10−10) surface) (right) heterostructures. Zn, O and Cu atoms are shown by grey, red and blue coloured balls, while small grey coloured balls depict H atoms.

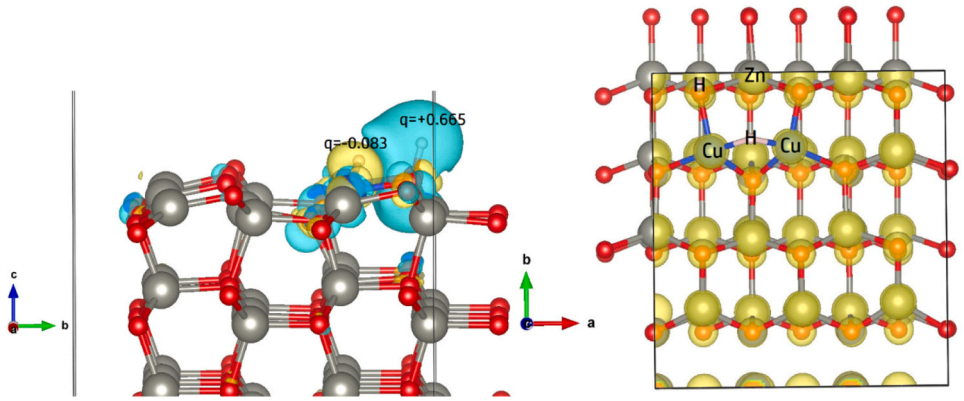

Fig. 11. Charge density difference plot of the H_2 molecule on the t-ZnO/CuO Hetero2 structure, where we have shown the Bader charge values of the hydrogen atoms (Left panel).

selectivity. Absolute selectivity for Hydrogen (100 ppm) at a maximum gas response (~550) was obtained from single microrod t-ZnO@CuO – based sensors. Dynamic investigations reveal a response time of ~17 s and a recovery time of ~89 s, attributed to the Arrhenius expression for conductivity. It's noteworthy that the sensor's performance is significantly influenced by the operating temperature. Overall, these studied nanostructures hold promise as both selective and sensitive hydrogen sensors, offering potential applications in various fields. As per we explore, t-ZnO@CuO core-shell microwire (single or two) structure with tetrapodal morphology of ZnO is a unique morphology for H_2 detection. To the best of our knowledge, this is the first time that a single microrod ZnO@CuO core-shell structure with better H_2 sensing response at

moderate temperature (150℃ or 175℃) has been shown. Complete coverage of CuO on t-ZnO tetrapod arms prevents large molecules from passing through and interacting at the interface which leads to excellent selectivity of H_2 molecules over VOCs (acetone, ethanol, methanol, or n-butanol) and ammonia. Computational analysis confirmed more coverage/substitution by Cu atoms (Hetero2 structure) are favourable interaction sites for H_2 molecules and reconfirmed by Bader charge analysis. This work covers experimental and computational aspects with special morphology for H_2 sensing at moderate temperature (175℃). The main novelty of the work is a new technological approach for nanoscale p-n heterostructure growing from amorphized nanoplatelets of CuO with t-ZnO microrods, which allows to fabricate single microrod t-ZnO@CuO – based sensors with absolute selectivity for H_2 over other VOC and significantly higher sensitivity, that is extremely important for green hydrogen industry.

Funding

Financial support by the project EU-project SENNET "Porous Networks for Gas Sensing", which runs under the Marie Skłodowska-Curie Actions funded by the European Union, under the number 101072845. This project was partially supported through the SERB SURE grant (SUR/2022/004935 year 2023) to A.K.M. at UPES. This paper was partially supported by the Technical University of Moldova and State Project: LIFETECH, No. 020404, Ministry of Education and Research.

CRediT authorship contribution statement

Nora de Leeuw: Validation, Software, Resources, Data curation. **Rainer Adelung:** Writing – review & editing, Validation, Supervision, Resources. **Oleg Lupan:** Writing – review & editing, Writing – original draft, Validation, Software, Project administration, Investigation, Funding acquisition, Conceptualization. **Leonard Siebert:** Writing – original draft, Visualization, Supervision, Project administration, Data curation, Conceptualization. **Barnika Chakraborty:** Validation, Methodology, Investigation, Formal analysis. **Dinu Litra:** Investigation, Formal analysis. **Abhishek Kumar Mishra:** Writing – review & editing, Writing – original draft, Visualization, Investigation, Data curation. **Cristian Lupan:** Writing – original draft, Software, Methodology, Investigation, Formal analysis. **Rajat Nagpal:** Methodology, Investigation, Formal analysis. **Soni Mishra:** Software, Project administration, Methodology. **Haoyi Qiu:** Validation, Software, Investigation. **Serghei Railean:** Supervision, Software, Data curation.

Declaration of Competing Interest

The authors declare that they have no known competing financial interests or personal relationships that could have appeared to influence the work reported in this paper.

Data availability

Data will be made available on request.

Acknowledgments

Financial support by the project EU-project SENNET "Porous Networks for Gas Sensing", which runs under the Marie Skłodowska-Curie Actions funded by the European Union, under the number 101072845. A.K.M. acknowledges the SERB SURE grant (SUR/2022/004935 year 2023) and SEED 2021 grant from UPES for computational facilities. This work used the ARCHER2 UK National Supercomputing Service (https://www.archer2.ac.uk). Partial support by State Project: LIFETECH, No. 020404 Ministry of Education and Research of Republic of Moldova.

Appendix A

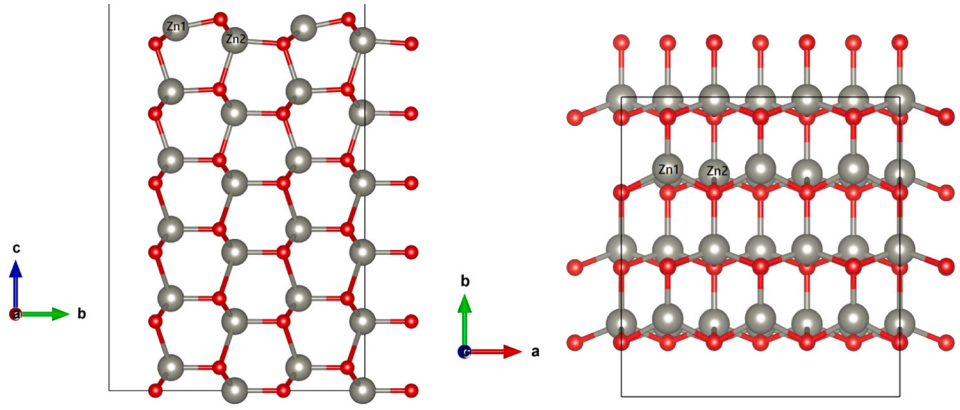

Figure A1. . 2×2 Supercell of ZnO(10−10) surface, where top and bottom images represent side and top views respectively. Zn and O atoms are shown by grey and red colored balls, respectively.

References

[1] H. Meixner, U. Lampe, Metal oxide sensors, Sens. Actuators B Chem. 33 (1996) 198–202, https://doi.org/10.1016/0925-4005(96)80098-0.
[2] J. Lenz, S. Edelstein, Magnetic sensors and their applications, IEEE Sens. J. 6 (2006) 631–649. ⟨https://doi.org/10.1109/JSEN.2006.874493⟩.
[3] H.-P. Loock, P.D. Wentzell, Detection limits of chemical sensors: applications and misapplications, Sens. Actuators B Chem. 173 (2012) 157–163, https://doi.org/10.1016/j.snb.2012.06.071.
[4] O. Lupan, N. Ababii, D. Santos-Carballal, M.-I. Terasa, N. Magariu, D. Zappa, E. Comini, T. Pauporté, L. Siebert, F. Faupel, A. Vahl, S. Hansen, N.H. de Leeuw, R. Adelung, Tailoring the selectivity of ultralow-power heterojunction gas sensors by noble metal nanoparticle functionalization, Nano Energy 88 (2021) 106241, https://doi.org/10.1016/j.nanoen.2021.106241.
[5] A. Dey, Semiconductor metal oxide gas sensors: a review, Mater. Sci. Eng. B 229 (2018) 206–217, https://doi.org/10.1016/j.mseb.2017.12.036.
[6] L. Cai, H. Li, H. Zhang, W. Fan, J. Wang, Y. Wang, X. Wang, Y. Tang, Y. Song, High Performance Gas Sensor Based on ZnO/CuO Heterostructures BT, in: Y. Peng, X. Dong (Eds.), Proceedings of 2019 International Conference on Optoelectronics and Measurement, Springer Singapore, Singapore, 2021, pp. 191–198.
[7] K.G. Motora, C.-M. Wu, G.M. Rani, W.-T. Yen, K.-S. Lin, Effect of electrode patterns on piezoelectric energy harvesting property of zinc oxide polyvinylidene fluoride based piezoelectric nanogenerator, Renew. Energy 217 (2023) 119208, https://doi.org/10.1016/j.renene.2023.119208.

[8] Y.K. Mishra, G. Modi, V. Cretu, V. Postica, O. Lupan, T. Reimer, I. Paulowicz, V. Hrkac, W. Benecke, L. Kienle, R. Adelung, Direct growth of freestanding ZnO tetrapod networks for multifunctional applications in photocatalysis, UV photodetection, and gas sensing, ACS Appl. Mater. Interfaces 7 (2015) 14303.
[9] D. Gedamu, I. Paulowicz, S. Kaps, O. Lupan, S. Wille, G. Haidarschin, Y.K. Mishra, R. Adelung, Rapid fabrication technique for interpenetrated ZnO nanotetrapod networks for fast UV sensors, Adv. Mater. 26 (2014) 1541–1550, https://doi.org/10.1002/adma.201304363.
[10] K.G. Motora, V.G. Dileepkumar, C.-M. Wu, R. Ashwini, G.-Y. Chen, M.S. Santosh, S. Kumar, D.-H. Kuo, Highly efficient and stable NiSe2-rGO composite-based room temperature hydrogen gas sensor, Int. J. Hydrogen Energy 50 (2024) 1174–1183, https://doi.org/10.1016/j.ijhydene.2023.10.018.
[11] B. Davis, D. Stuart, M. Nieves Maldonado, V. Kamavaram, Q. Cheng, V. Veedu, Intelligent Hydrogen Gas Monitoring in Natural Gas/Hydrogen Blending, in: Day 3 Wed, May 04, 2022, OTC, 2022: p. D031S034R003. https://doi.org/10.4043/32007-MS.
[12] L. Kékedy-Nagy, M. Abolhassani, S.I. Perez Bakovic, Z. Anari, J.P. Moore II, B. G. Pollet, L.F. Greenlee, Electroless production of fertilizer (Struvite) and hydrogen from synthetic agricultural wastewaters, J. Am. Chem. Soc. 142 (2020) 18844–18858, https://doi.org/10.1021/jacs.0c07916.
[13] L. Mosca, E. Palo, M. Colozzi, G. Iaquaniello, A. Salladini, S. Taraschi, Hydrogen in chemical and petrochemical industry, in: A. Iulianelli, A. Basile (Eds.), Curr. Trends Futur. Dev. Membr., 17, Elsevier, 2020, pp. 387–410, https://doi.org/10.1016/B978-0-12-817384-8.00017-0.
[14] M. Granovskii, I. Dincer, M.A. Rosen, Greenhouse gas emissions reduction by use of wind and solar energies for hydrogen and electricity production: Economic factors, Int. J. Hydrogen Energy 32 (2007) 927–931, https://doi.org/10.1016/j.ijhydene.2006.09.029.
[15] F.J. Recio, M.C. Alonso, L. Gaillet, M. Sánchez, Hydrogen embrittlement risk of high strength galvanized steel in contact with alkaline media, Corros. Sci. 53 (2011) 2853–2860, https://doi.org/10.1016/j.corsci.2011.05.023.
[16] BSI Standards Publication Safety requirements for secondary batteries and battery installations Part 1: General safety information, (2010).
[17] K. Motora, C. Wu, G. Rani, W.-T. Yen, Effect of ZnO particle size on piezoelectric nanogenerators and mechanical energy harvesting, Express Polym. Lett. 16 (2022) 1208–1227, https://doi.org/10.3144/expresspolymlett.2022.88.
[18] C.-M. Shrisha, K.G. Wu, G.-Y. Motora, J.P. Chen, Y. Chu, H.-H. Cheng, Hsu, Development of p-type zinc oxide nanorods on zirconium-based metallic glass nanotube arrays by facile hydrothermal method for gas sensing applications, Chem. Eng. J. 463 (2023) 142381, https://doi.org/10.1016/j.cej.2023.142381.
[19] T. Hübert, L. Boon-Brett, G. Black, U. Banach, Hydrogen sensors – a review, Sens. Actuators B Chem. 157 (2011) 329–352, https://doi.org/10.1016/j.snb.2011.04.070.
[20] I. Darmadi, F.A.A. Nugroho, C. Langhammer, High-performance nanostructured palladium-based hydrogen sensors—current limitations and strategies for their mitigation, ACS Sens. 5 (2020) 3306–3327, https://doi.org/10.1021/acssensors.0c02019.
[21] X. Wang, L. Du, L. Cheng, S. Zhai, C. Zhang, W. Wang, Y. Liang, D. Yang, Q. Chen, G. Lei, Pd/Ni nanowire film coated SAW hydrogen sensor with fast response, Sens. Actuators B Chem. 351 (2022) 130952, https://doi.org/10.1016/j.snb.2021.130952.
[22] H. Farahani, R. Wagiran, M. Hamidon, Humidity sensors principle, mechanism, and fabrication technologies: a comprehensive review, Sensors 14 (2014) 7881–7939, https://doi.org/10.3390/s140507881.
[23] O. Lupan, Analysis of ZnO-nanorods grown on p-Si (100) via catalystfree hydrothermal deposition, Meridian Ing. (2011) 31–36.
[24] D.R. Miller, S.A. Akbar, P.A. Morris, Nanoscale metal oxide-based heterojunctions for gas sensing: a review, Sens. Actuators B Chem. 204 (2014) 250–272, https://doi.org/10.1016/j.snb.2014.07.074.
[25] N. Datta, N. Ramgir, M. Kaur, S. Kailasa Ganapathi, A.K. Debnath, D.K. Aswal, S. K. Gupta, Selective H2S sensing characteristics of hydrothermally grown ZnO-nanowires network tailored by ultrathin CuO layers, Sens. Actuators B Chem. 166–167 (2012) 394–401, https://doi.org/10.1016/j.snb.2012.02.079.
[26] A. Moumen, G.C.W. Kumarage, E. Comini, P-type metal oxide semiconductor thin films: synthesis and chemical sensor applications, Sensors 22 (2022), https://doi.org/10.3390/s22041359.
[27] Y.-H. Choi, D.-H. Kim, S.-H. Hong, K.S. Hong, H2 and C2H5OH sensing characteristics of mesoporous p-type CuO films prepared via a novel precursor-based ink solution route, Sens. Actuators B Chem. 178 (2013) 395–403, https://doi.org/10.1016/j.snb.2012.12.096.
[28] O. Lupan, V. Cretu, V. Postica, O. Polonskyi, N. Ababii, F. Schütt, V. Kaidas, F. Faupel, R. Adelung, Non-planar nanoscale p–p heterojunctions formation in ZnxCu1−xOy nanocrystals by mixed phases for enhanced sensors, Sens. Actuators B Chem. 230 (2016) 832–843, https://doi.org/10.1016/j.snb.2016.02.089.
[29] K. Kumar, R.R. Kakarla, V. Sadhu, N. Shetti, C. Reddy, R. Chouhan, S. Naveen, Metal oxide-based nanosensors for healthcare and environmental applications, in: 2020: pp. 113–129. https://doi.org/10.1016/B978-0-12-817923-9.00004-3.
[30] H.-J. Kim, J.-H. Lee, Highly sensitive and selective gas sensors using p-type oxide semiconductors: overview, Sens. Actuators B Chem. 192 (2014) 607–627, https://doi.org/10.1016/j.snb.2013.11.005.
[31] E. Fortunato, P. Barquinha, R. Martins, Oxide semiconductor thin-film transistors: a review of recent advances, Adv. Mater. 24 (2012) 2945–2986, https://doi.org/10.1002/adma.201103228.
[32] Y.K. Mishra, S. Kaps, A. Schuchardt, I. Paulowicz, X. Jin, D. Gedamu, S. Freitag, M. Claus, S. Wille, A. Kovalev, S.N. Gorb, R. Adelung, Ceramics: fabrication of macroscopically flexible and highly porous 3D semiconductor networks from interpenetrating nanostructures by a simple flame transport approach, Part. Part. Syst. Charact. 30 (2013) 731–731, https://doi.org/10.1002/ppsc.201370034.
[33] O. Lupan, L. Chow, G. Chai, L. Chernyak, O. Lopatiuk-Tirpak, H. Heinrich, Focused-ion-beam fabrication of ZnO nanorod-based UV photodetector using the in-situ lift-out technique, Phys. Status Solidi 205 (2008) 2673–2678, https://doi.org/10.1002/pssa.200824233.
[34] G. Kresse, J. Hafner, Ab initio molecular dynamics for liquid metals, Phys. Rev. B Condens. Matter Mater. Phys. 47 (1993) 558.
[35] G. Kresse, J. Furthmüller, Efficient iterative schemes for ab initio total-energy calculations using a plane-wave basis set, Phys. Rev. B Condens. Matter Mater. Phys. 54 (1996) 11169.
[36] G. Kresse, J. Furthmüller, Efficiency of ab initio total-energy calculations for metals and semiconductors using a plane-wave basis set, Comput. Mater. Sci. 6 (1996) 15.
[37] G. Kresse, J. Hafner, Ab initio molecular-dynamics simulation of the liquid-metal–amorphous-semiconductor transition in germanium, Phys. Rev. B Condens. Matter Mater. Phys. 49 (1994) 14251.
[38] P.E. Blöchl, Projector augmented-wave method, Phys. Rev. B Condens. Matter Mater. Phys. 50 (1994) 17953.
[39] J.P. Perdew, K. Burke, M. Ernzerhof, Generalized gradient approximation made simple, Phys. Rev. Lett. 77 (1996) 3865.
[40] P.E. Blöchl, O. Jepsen, O.K. Andersen, Improved tetrahedron method for brillouin-zone integrations, Phys. Rev. B Condens. Matter Mater. Phys. 49 (1994) 16223.
[41] H.J. Monkhorst, J.D. Pack, Special points for brillouin-zone integrations, Phys. Rev. B 13 (1976) 5188.
[42] O. Lupan, V. Postica, J. Gröttrup, A.K. Mishra, N.H. de Leeuw, J.F.C. Carreira, J. Rodrigues, N. Ben Sedrine, M.R. Correia, T. Monteiro, V. Cretu, I. Tiginyanu, D. Smazna, Y.K. Mishra, R. Adelung, Hybridization of zinc oxide tetrapods for selective gas sensing applications, ACS Appl. Mater. Interfaces 9 (2017) 4084–4099, https://doi.org/10.1021/acsami.6b11337.
[43] O. Lupan, D. Santos-Carballal, N. Magariu, A.K. Mishra, N. Ababii, H. Krüger, N. Wolff, A. Vahl, M.T. Bodduluri, N. Kohlmann, L. Kienle, R. Adelung, N.H. de Leeuw, S. Hansen, Al2O3/ZnO heterostructure-based sensors for volatile organic compounds in safety applications, ACS Appl. Mater. Interfaces 14 (2022) 29331–29344, https://doi.org/10.1021/acsami.2c03704.
[44] C. Lupan, A.K. Mishra, N. Wolff, J. Drewes, H. Krüger, A. Vahl, O. Lupan, T. Pauporté, B. Viana, L. Kienle, R. Adelung, N.H. de Leeuw, S. Hansen, Nanosensors based on a single ZnO:Eu nanowire for hydrogen gas sensing, ACS Appl. Mater. Interfaces 14 (2022) 41196–41207, https://doi.org/10.1021/acsami.2c10975.
[45] S. Grimme, J. Antony, S. Ehrlich, H. Krieg, A consistent and accurate ab initio parametrization of density functional dispersion correction (DFT-D) for the 94 elements H-Pu, J. Chem. Phys. 132 (2010) 154104, https://doi.org/10.1063/1.3382344.
[46] G. Henkelman, A. Arnaldsson, H. Jónsson, A fast and robust algorithm for Bader decomposition of charge density, Comput. Mater. Sci. 36 (2006) 354–360, https://doi.org/10.1016/j.commatsci.2005.04.010.
[47] M. Hoppe, O. Lupan, V. Postica, N. Wolff, V. Duppel, L. Kienle, I. Tiginyanu, R. Adelung, ZnAl2O4-functionalized zinc oxide microstructures for highly selective hydrogen gas sensing applications, Phys. Status Solidi 215 (2018) 1700772, https://doi.org/10.1002/pssa.201700772.
[48] B. Giraldo, W. Yeh, N.P. Kobayashi, Formation of single-crystal Cu2O strips in non-single-crystal CuO thin films by continuous-wave laser diode with micro-chevron laser beam ($$\mu$$-CLB), J. Mater. Sci. 55 (2020) 14105–14111. https://doi.org/10.1007/s10853-020-05013-7.
[49] R.F. Zhuo, H.T. Feng, J.T. Chen, D. Yan, J.J. Feng, H.J. Li, B.S. Geng, S. Cheng, X. Y. Xu, P.X. Yan, Multistep synthesis, growth mechanism, optical, and microwave absorption properties of ZnO dendritic nanostructures, J. Phys. Chem. C 112 (2008) 11767–11775, https://doi.org/10.1021/jp804090q.
[50] P.S. Murthy, V.P. Venugopalan, D.A. Das, S. Dhara, R. Pandiyan, A.K. Tyagi, Antibiofilm activity of nano sized CuO, in: Int. Conf. Nanosci. Eng. Technol. (ICONSET 2011), IEEE, 2011: pp. 580–583. https://doi.org/10.1109/ICONSET.2011.6168037.
[51] S. Schröder, N. Ababii, O. Lupan, J. Drewes, N. Magariu, H. Krüger, T. Strunskus, R. Adelung, S. Hansen, F. Faupel, Sensing performance of CuO/Cu2O/ZnO:Fe heterostructure coated with thermally stable ultrathin hydrophobic PV3D3 polymer layer for battery application, Mater. Today Chem. 23 (2022) 100642, https://doi.org/10.1016/j.mtchem.2021.100642.
[52] P. Kutukov, M. Rumyantseva, V. Krivetskiy, D. Filatova, M. Batuk, J. Hadermann, N. Khmelevsky, A. Aksenenko, A. Gaskov, Influence of mono- and bimetallic PtOx, PdOx, PtPdOx clusters on CO sensing by SnO2 based gas sensors, Nanomaterials 8 (2018), https://doi.org/10.3390/nano8110917.
[53] N. Yamazoe, K. Suematsu, K. Shimanoe, Extension of receptor function theory to include two types of adsorbed oxygen for oxide semiconductor gas sensors, Sens. Actuators B Chem. 163 (2012) 128–135, https://doi.org/10.1016/j.snb.2012.01.020.
[54] N. Ma, K. Suematsu, M. Yuasa, T. Kida, K. Shimanoe, Effect of water vapor on Pd-loaded SnO2 nanoparticles gas sensor, ACS Appl. Mater. Interfaces 7 (2015) 5863–5869, https://doi.org/10.1021/am509082w.
[55] K. Großmann, S. Wicker, U. Weimar, N. Barsan, Impact of Pt additives on the surface reactions between SnO2, water vapour, CO and H2; an operando investigation, Phys. Chem. Chem. Phys. 15 (2013) 19151–19158, https://doi.org/10.1039/C3CP52782D.
[56] Y. Yang, S. Kim, K. Kim, D.G. Jung, D. Jung, Enhanced hydrogen gas sensing characteristics of CuO/ZnO heterojunction for thickness-dependence and its application, Surf. Interfaces 46 (2024) 104131, https://doi.org/10.1016/j.surfin.2024.104131.

[57] N. Ababii, V. Postica, M. Hoppe, R. Adelung, O. Lupan, S. Railean, T. Pauporté, B. Viana, H2 gas sensing properties of a ZnO/CuO and ZnO/CuO/Cu2O Heterostructures, in: F.H. Teherani, D.C. Look, D.J. Rogers (Eds.), Proc. SPIE, 2017: p. 101052A. ⟨https://doi.org/10.1117/12.2253153⟩.
[58] U. Hoefer, J. Frank, M. Fleischer, High temperature Ga2O3-gas sensors and SnO2-gas sensors: a comparison, Sens. Actuators B Chem. 78 (2001) 6–11, https://doi.org/10.1016/S0925-4005(01)00784-5.
[59] G. Jiménez-Cadena, J. Riu, F.X. Rius, Gas sensors based on nanostructured materials, Analyst 132 (2007) 1083–1099, https://doi.org/10.1039/B704562J.
[60] N. Yamazoe, G. Sakai, K. Shimanoe, Oxide semiconductor gas sensors, Catal. Surv. Asia 7 (2003) 63–75, https://doi.org/10.1023/A:1023436725457.
[61] G. Kiss, O.H. Krafcsik, K. Kovács, V.K. Josepovits, M. Fleischer, H. Meixner, P. Deák, F. Réti, Impedance spectroscopic and secondary ion mass spectrometric studies of β-Ga2O3/O2 interaction, Thin Solid Films 391 (2001) 239–242, https://doi.org/10.1016/S0040-6090(01)00988-9.
[62] H.-J. Lin, J.P. Baltrus, H. Gao, Y. Ding, C.-Y. Nam, P. Ohodnicki, P.-X. Gao, Perovskite nanoparticle-sensitized Ga 2 O 3 nanorod arrays for CO detection at high temperature, ACS Appl. Mater. Interfaces 8 (2016) 8880–8887, https://doi.org/10.1021/acsami.6b01709.
[63] K. Malook, H. Khan, M. Ali, Ihsan-Ul-Haque, Investigation of room temperature humidity sensing performance of mesoporous CuO particles, Mater. Sci. Semicond. Process. 113 (2020) 105021, https://doi.org/10.1016/j.mssp.2020.105021.
[64] C. Prakash, R. Chaurasiya, A.J. Kale, A. Dixit, Low-temperature highly robust hydrogen sensor using pristine ZnO nanorods with enhanced response and selectivity, ACS Omega 7 (2022) 28206–28216, https://doi.org/10.1021/acsomega.2c02510.
[65] C. Lupan, V. Crețu, A.K. Mishra, N. Magariu, N. Manciu, N. Ababii, S. Mishra, S. Railean, L. Zimoch, V. Galstyan, S. Hansen, T. Pauporté, Thin films of copper oxide nanostructured via rapid thermal processing, J. Eng. Sci. 29 (2023) 84–96, https://doi.org/10.52326/jes.utm.2022.29(4).04.
[66] S. Aygün, D. Cann, Hydrogen sensitivity of doped CuO/ZnO heterocontact sensors, Sens. Actuators B-Chem. 106 (2005) 837–842. ⟨https://doi.org/10.1016/j.snb.2004.10.004⟩.
[67] N. Yamazoe, K. Shimanoe, Basic approach to the transducer function of oxide semiconductor gas sensors, Sens. Actuators B Chem. 160 (2011) 1352–1362, https://doi.org/10.1016/j.snb.2011.09.075.
[68] L. Siebert, N. Wolff, N. Ababii, M.-I. Terasa, O. Lupan, A. Vahl, V. Duppel, H. Qiu, M. Tienken, M. Mirabelli, V. Sontea, F. Faupel, L. Kienle, R. Adelung, Facile fabrication of semiconducting oxide nanostructures by direct ink writing of readily available metal microparticles and their application as low power acetone gas sensors, Nano Energy 70 (2020) 104420, https://doi.org/10.1016/j.nanoen.2019.104420.
[69] O. Lupan, V. Postica, N. Ababii, M. Hoppe, V. Cretu, I. Tiginyanu, V. Sontea, T. Pauporté, B. Viana, R. Adelung, Influence of CuO nanostructures morphology on hydrogen gas sensing performances, Microelectron. Eng. 164 (2016) 63–70, https://doi.org/10.1016/j.mee.2016.07.008.
[70] M. Sadeghian Lemraski, E. Nadimi, Acetone gas sensing mechanism on zinc oxide surfaces: a first principles calculation, Surf. Sci. 657 (2017) 96–103, https://doi.org/10.1016/j.susc.2016.11.013.
[71] L. Siebert, O. Lupan, M. Mirabelli, N. Ababii, M.-I. Terasa, S. Kaps, V. Cretu, A. Vahl, F. Faupel, R. Adelung, 3D-printed chemiresistive sensor array on nanowire CuO/Cu 2 O/Cu heterojunction nets, ACS Appl. Mater. Interfaces 11 (2019) 25508–25515, https://doi.org/10.1021/acsami.9b04385.
[72] O. Lupan, G. Chai, L. Chow, Novel hydrogen gas sensor based on single ZnO nanorod, Microelectron. Eng. 85 (2008) 2220–2225, https://doi.org/10.1016/j.mee.2008.06.021.
[73] O. Lupan, V.V. Ursaki, G. Chai, L. Chow, G.A. Emelchenko, I.M. Tiginyanu, A. N. Gruzintsev, A.N. Redkin, Selective hydrogen gas nanosensor using individual ZnO nanowire with fast response at room temperature, Sens. Actuators B Chem. 144 (2010) 56–66, https://doi.org/10.1016/j.snb.2009.10.038.
[74] R. Yatskiv, S. Tiagulskyi, J. Grym, J. Vaniš, N. Bašinová, P. Horak, A. Torrisi, G. Ceccio, J. Vacik, M. Vrňata, Optical and electrical characterization of CuO/ZnO heterojunctions, Thin Solid Films 693 (2020) 137656, https://doi.org/10.1016/j.tsf.2019.137656.
[75] N. Ababii, T. Reimer, V. Postica, M. Hoppe, S. Chemnitz, V. Shontya, W. Benecke, R. Adelung, O. Lupan, Influence of TiO2 ultra-thin films on gas sensing properties of CuO: Zn, Microelectron. Comput. Sci. (2017) 33–34.